Supplementary Material

Au-modified Cu_2O nanocubes for light-enhanced nitrate electroreduction to ammonia

Yi-Ting Yang,[a] Xiao-Hui Wang,[a] Ze-Nong Zhang,[a] Xuan Ai,[b] Xue Xiao,[b]* Yu Chen,[b]* and Shu-Ni Li[a]*

[a] *Key Laboratory of Macromolecular Science of Shaanxi Province, School of Chemistry and Chemical Engineering, Shaanxi Normal University, Xi'an 710062, PR China.*

[b] *School of Materials Science and Engineering, Shaanxi Normal University, Xi'an 710062, PR China.*

*Corresponding authors

E-mail addresses: tiffanyxx110@gmail.com (X. Xiao), ndchenyu@gmail.com (Y. Chen) and lishuni@snnu.edu.cn (S.-N. Li)

Reagents and chemicals

Copper chloride dehydrate ($CuCl_2 \cdot 2H_2O$), potassium nitrate (KNO_3, 99 %), sodium hydroxide (NaOH, 97 %), potassium sulfate (K_2SO_4), L-ascorbic acid ($C_6H_8O_6$), chloroauric acid ($HAuCl_4$), sodium borohydride ($NaBH_4$), and ethylene glycol ($C_2H_6O_2$) are purchased from Aladdin Industrial Corporation (Shanghai, China).

Physical characterization

The powder X-ray diffraction (XRD) patterns were acquired by an X−ray diffractometer (DX-2700) with Cu Kα radiation. Energy dispersive X-ray spectroscopy (EDX) was obtained at Quanta 200. The morphology and microstructures were analyzed by scanning electron microscopy (SEM, Tecnai G2 F20), transmission electron microscopy (TEM, TECNAI G2 F20). Electronic information was investigated by X-ray photoelectron spectroscopy (XPS, AXIS ULTRA), and the binding energy was calibrated with a C 1s peak of 284.6 eV as the standard value. UV-visible spectrometer (UV-vis) data were obtained at a Lambda 1050 spectrometer. ^{1}H NMR spectra were measured by nuclear magnetic resonance (NMR) measurement (Bruker 400-MHz system).

Electrochemical measurements

All electrochemical experiments were performed on an electrochemical workstation (CHI 660E) at 30 ℃ using different electrochemical testing techniques,

such as linear sweep voltammetry (LSV), cyclic voltammetry (CV), chronoamperometry (i-t) and electrochemical impedance spectroscopy (EIS). In the standard three-electrode system, the graphite electrode was used as the counter electrode, the saturated calomel electrode (SCE) was used as the reference electrode, and the glassy carbon electrode containing an electrocatalyst was used as the working electrode. All potentials in this work were calibrated using a reversible hydrogen electrode (RHE, $E_{RHE} = E_{SCE} + 0.242\ V + 0.0591\ pH$). The electrocatalysts ink (2 mg mL^{-1}) was formed by dispersing 2 mg of catalyst into 1 mL of mixed solvent (H_2O + isopropanol, V_1/V_2= 8:2) and 10 μL Nafion solution (5 wt %). Then, 4 μL of electrocatalysts ink was dropped on the glassy carbon electrode (3 mm diameter) and dried at room temperature.

The Faradaic efficiency of NO_3^-RR and NH_3 yield

The Faraday efficiency of NO_3^- to NH_3 could be calculated by the following formula:

$$FE_{NH_3} = (8 \times F \times c_{NH_3} \times V)/(17 \times Q)$$

The NH_3 yield could be calculated by the following formula:

$$Yield_{NH_3} = (c_{NH_3} \times V)/(m \times t)$$

The Faraday efficiency of NO_2^- to NH_3 could be calculated by the following formula:

$$FE_{NO_2^-} = (2 \times F \times c_{NO_2^-} \times V)/(46 \times Q)$$

The NO_2^- yield could be calculated by the following formula:

$$\text{Yield}_{NO_2^-} = (c_{NO_2^-} \times V)/(m \times t)$$

$c_{NH_3}$was the mass concentration of NH_3 (aq), V was the volume of electrolyte in the cathode compartment (20 mL), t was the electrolytic time (3 h), F was the Faradaic constant (96485 C mol^{-1}), Q was the total charge passing the electrode, m and t were the electrocatalyst mass and the reduction reaction time, respectively.

Determination of NH_3 concentration

The NH_3 concentration was determined by the phenol-hypochlorite method. The standard curve was drawn as follows: Dry the solid of $(NH_4)_2SO_4$ at 120 ℃ for 2 h in advance. A series of standard ammonium sulfate solutions were prepared, and 0.4 mL phenol alcohol, 0.4 mL $Na_2[Fe(CN)_5NO]$ and 1 mL oxidizing agent were added to 10 mL standard solution of different concentrations successively. After mixing well, the solution was placed in the dark for 3 h. The absorption spectrum was measured by using a UV-vis spectrophotometer in the range of 500-800 nm.

After running the chronoamperometry test for 3 h, 1 mL electrolyte was diluted to 10 mL with water. The absorbance of the solution was measured by the same experimental method as the standard curve, and calculated the NH_4^+-N concentration (c_{NH_3}) according to the UV-vis curve and the standard curve.

Determination of nitrite

The concentration of NO_2^- was detected by the N-(1-naphthyl) ethylenediamine spectrophotometry method. Take 1.0 mL electrolyte in a 50 mL volumetric bottle, dilute it with a little deionized water, then add 1.0 mL p-aminobenzenesulfonamide and mix well. After leaving for 2-8 min, add 1.0 mL N-(1-naphthyl) ethylenediamine dihydrochloride and mix well. After 10 min, the absorbance was measured by a UV-vis spectrophotometer at 540 nm wavelength. The concentration-absorbance curve was made using a series of standard sodium nitrite solutions.

^{15}N and ^{14}N isotope labeling experiments

Isotope labeling experiments were performed to confirm the source of NH_4^+-N using $K^{15}NO_3$ and $K^{14}NO_3$ as the original nitrogen source, respectively.

Figure section

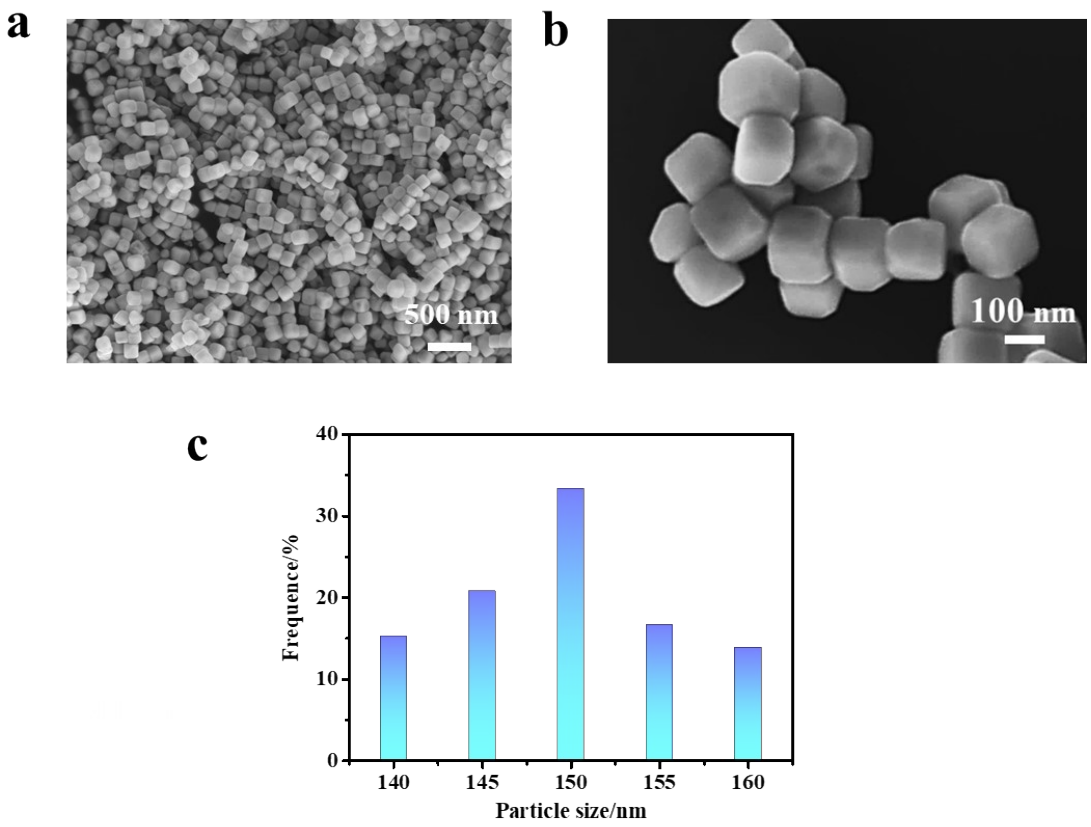

Fig. S1. (a-b) SEM images and (c) particle size distribution histograms of Cu_2O NCs.

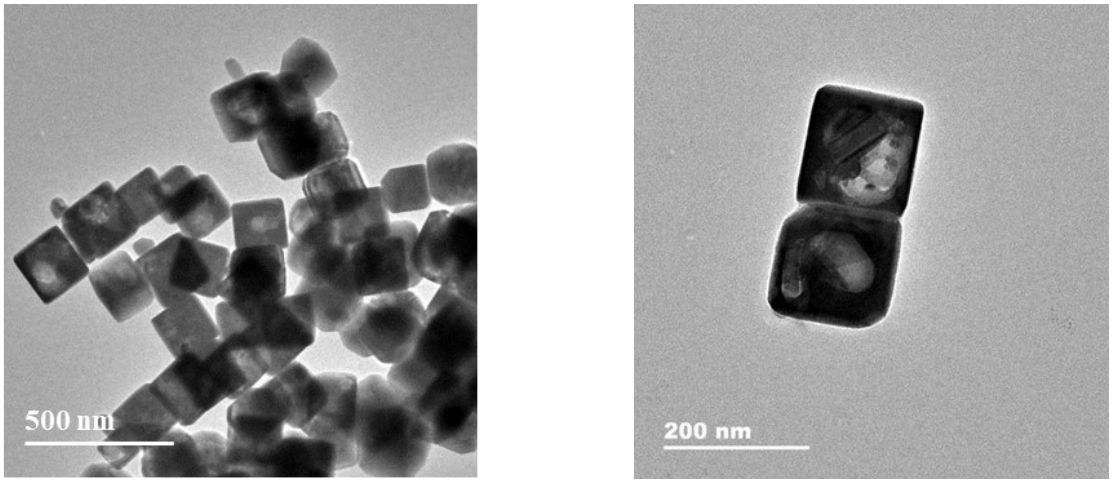

Fig. S2. TEM images of Cu_2O NCs.

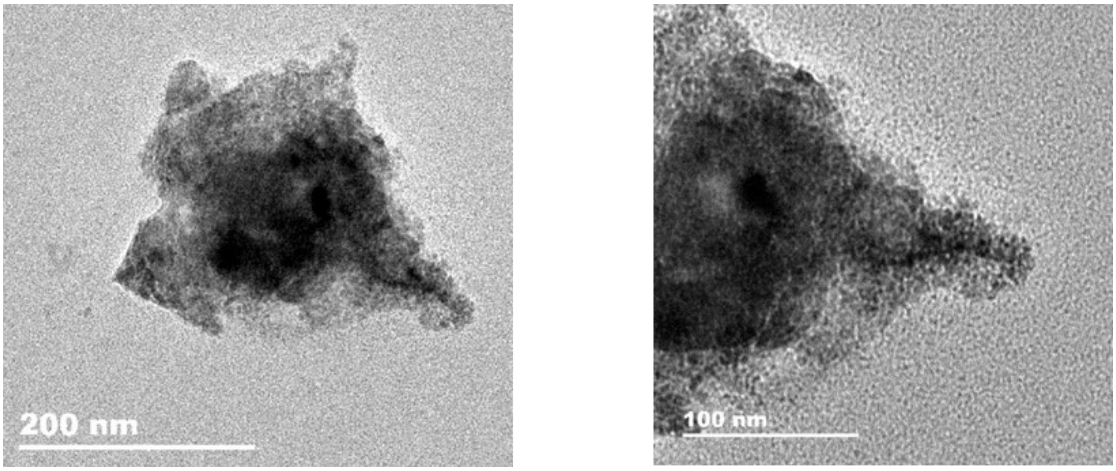

Fig. S3. TEM images of Au NPs.

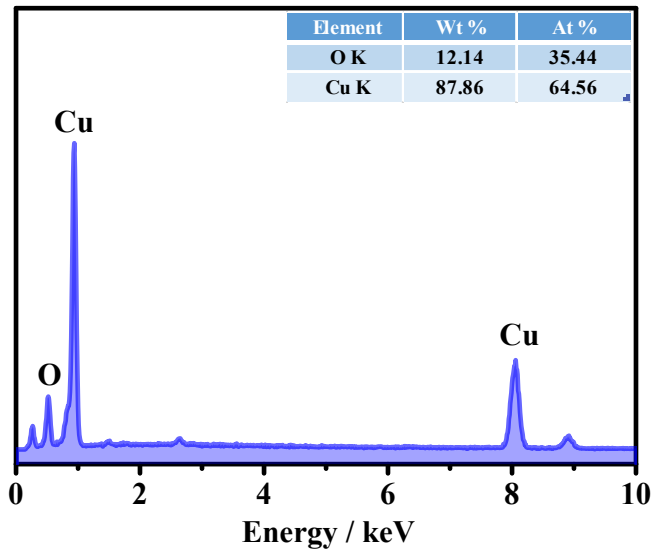

Fig. S4. EDX spectrum of Cu_2O NCs.

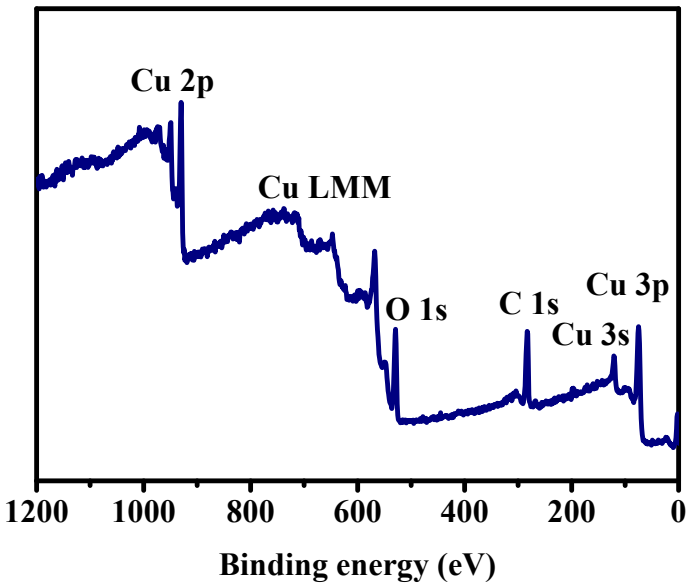

Fig. S5. Full XPS spectrum of Cu_2O NCs.

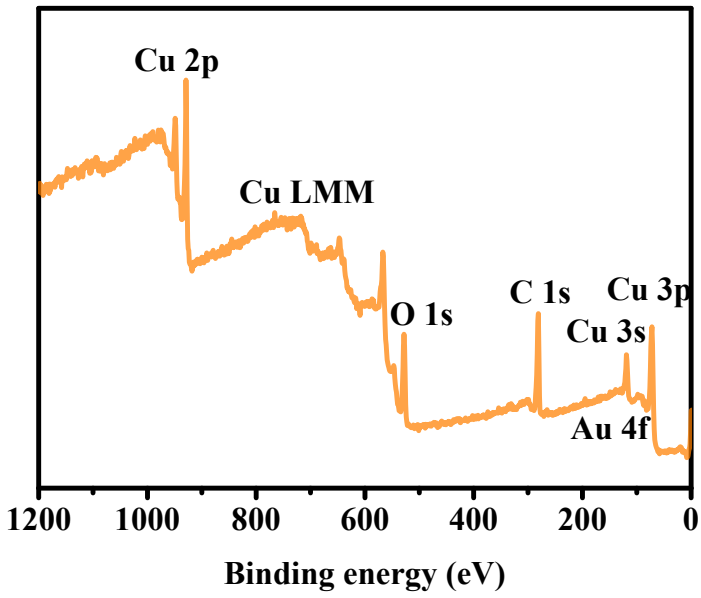

Fig. S6. Full XPS spectrum of Au/Cu_2O NCs.

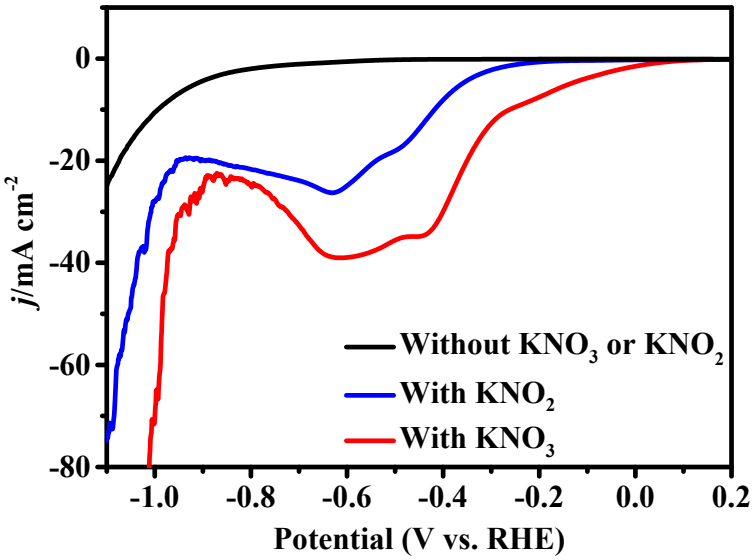

Fig. S7. LSV curves of Au/Cu_2O NCs in 0.5 M K_2SO_4 electrolyte with KNO_3 and KNO_2 at 10 mV s^{-1}.

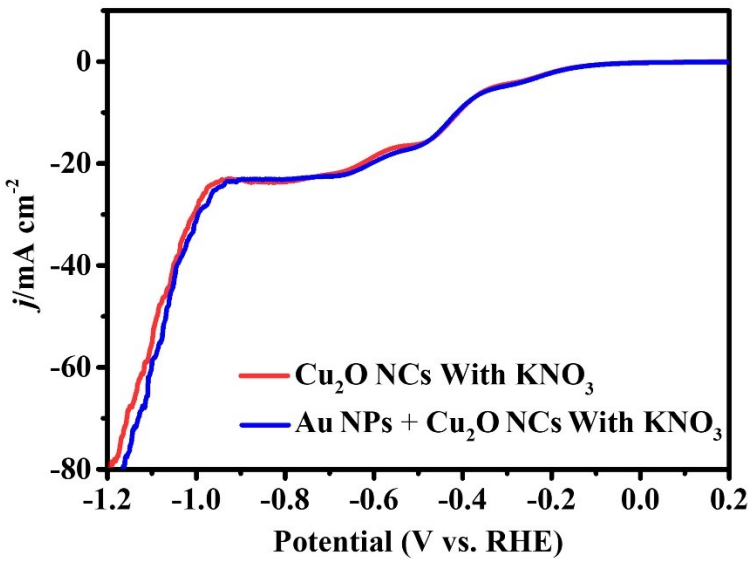

Fig. S8 The LSV curves of Cu_2O (red line) and Au NPs + Cu_2O (blue line) for NO_3^- RR.

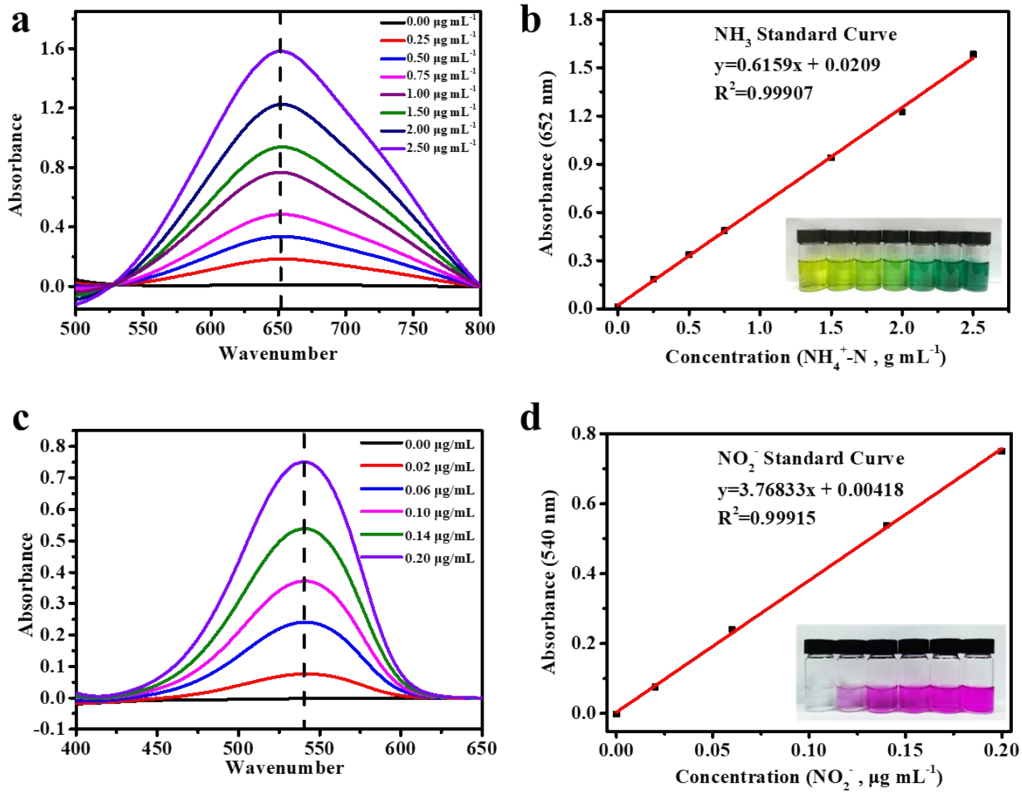

Fig. S9. (a) UV-vis adsorption curves and (b) calibration curves of NH_4^+-N. (c) UV-vis adsorption curves and (d) calibration curves of NO_2^-.

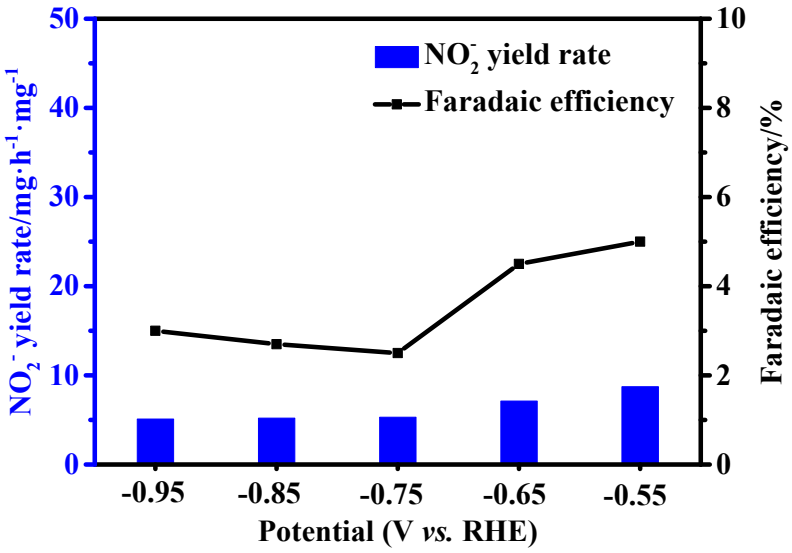

Fig. S10. The Faradaic efficiency and NO_2^- yield on Au/Cu_2O NCs at different potentials.

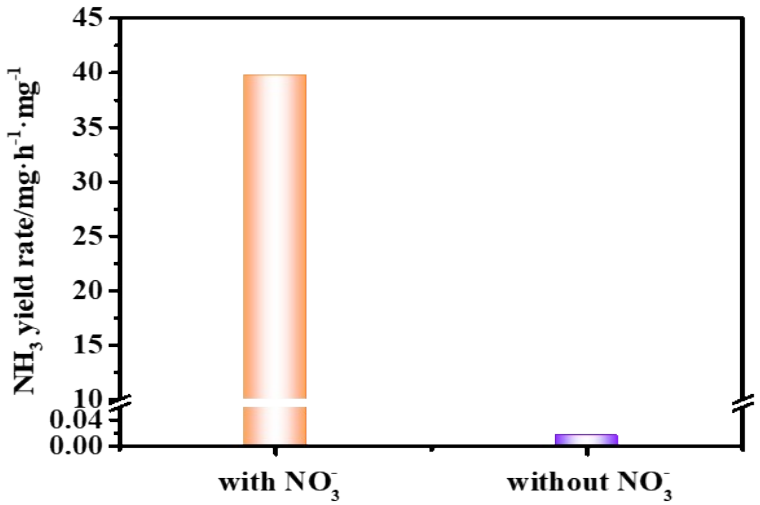

Fig. S11. The NH_3 yield on Au/Cu_2O NCs in 0.5 M K_2SO_4 electrolyte with and without NO_3^-.

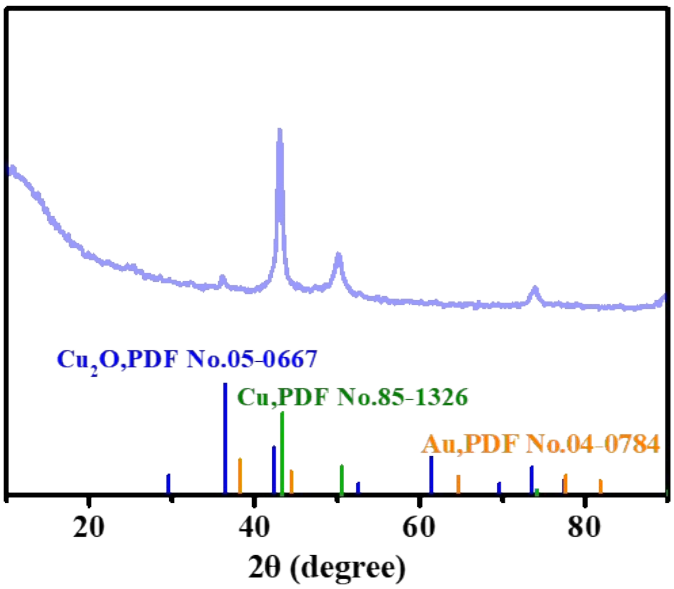

Fig. S12. XRD pattern of Au/Cu_2O NCs after chronoamperometry test.

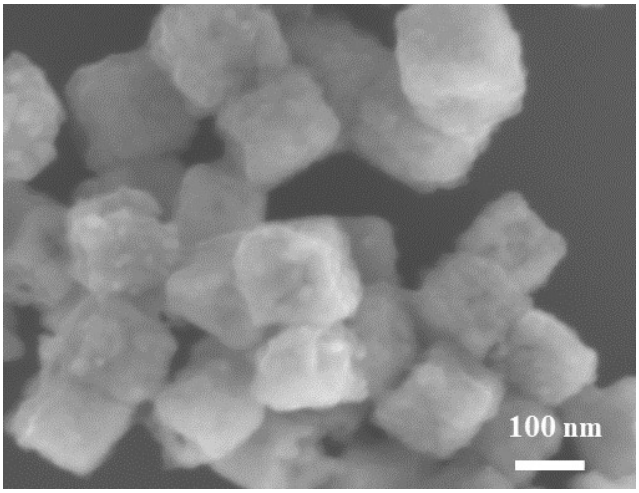

Fig. S13. SEM image of Au/Cu_2O NCs after chronoamperometry test.

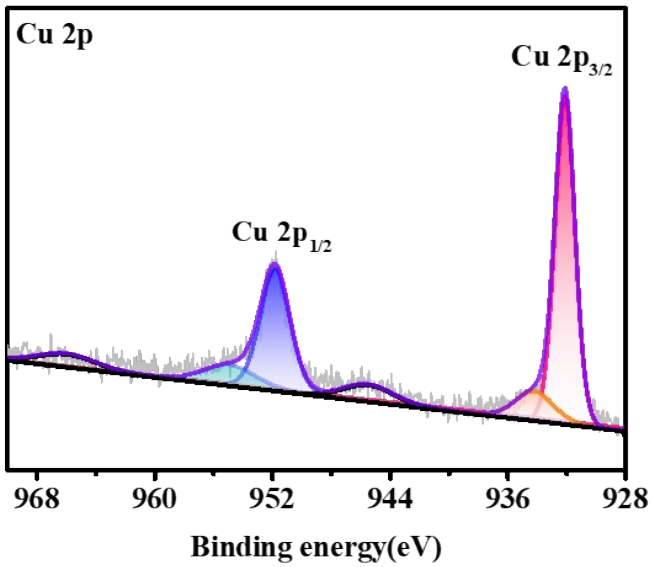

Fig. S14. Cu 2p XPS spectrum of Au/Cu_2O NCs after chronoamperometry test.

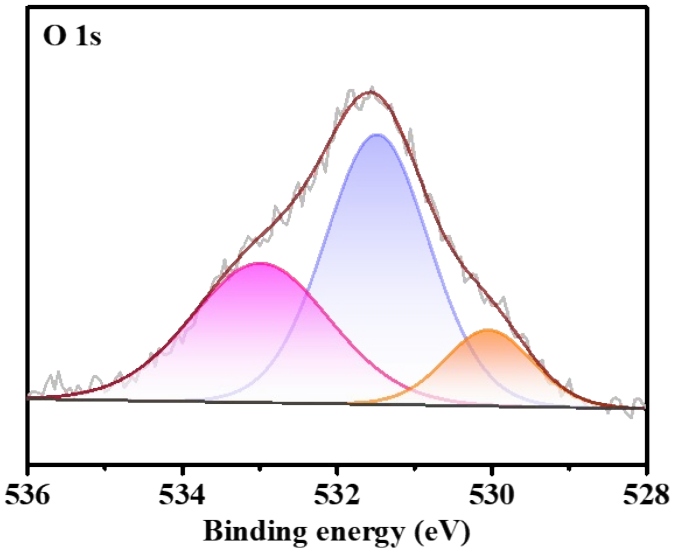

Fig. S15. O 1s XPS spectrum of Au/Cu_2O NCs after chronoamperometry test.

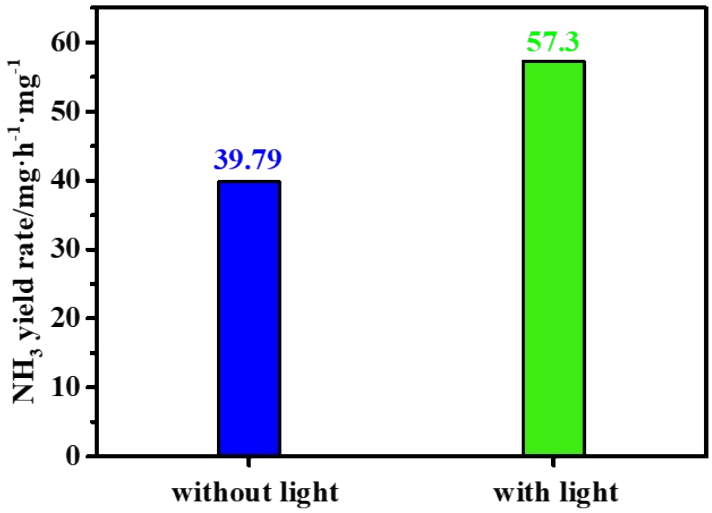

Fig. S16. NH_3 yield of Au/Cu_2O NCs with/without light.

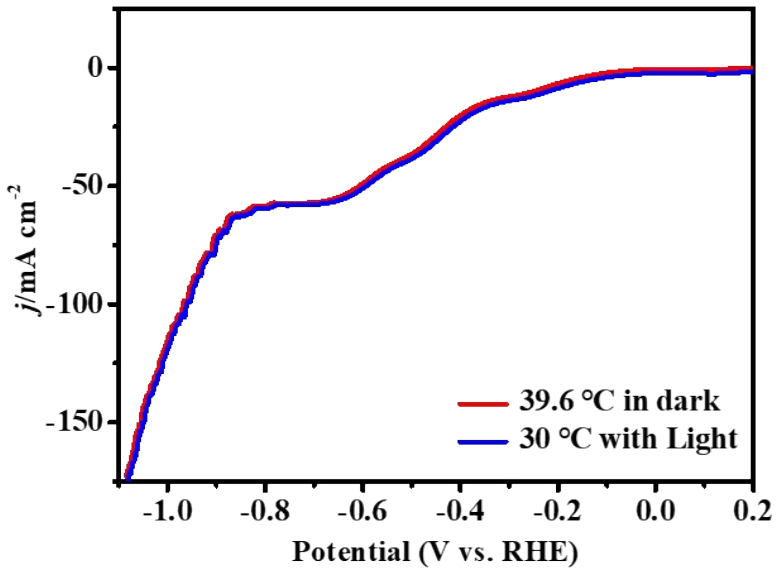

Fig. S17. LSV curves of Au/Cu_2O NCs at 30 ℃ with light and 39.6 ℃ in dark.

Table S1. The comparison of NO_3^-RR performance between Au/Cu_2O NCs and some other reported electrocatalysts.

Electrocatalysts	Electrolyte	NH_3 yield	Faradaic Efficiency (%)	Ref. (year)
Au/Cu_2O NCs	**0.5 M K_2SO_4 50 mM KNO_3**	**39.79 mg h^{-1} mg_{cat}^{-1}**	**92.93**	**This work**
Co_1-P co-doped graphitic carbon	0.5 M Na_2SO_4 0.1 M KNO_3	8.6 mg h^{-1} mg_{cat}^{-1}	93.8	2024[1]
Cu_xO/N-doped graphdiyne	0.1 M KOH 0.1 M KNO_3	5.78 mg h^{-1} mg_{cat}^{-1}	85	2024[2]
Cu/Cu_2O/Pi nanowires	1 M KOH 0.1 M KNO_3	20.475 mg h^{-1} mg_{cat}^{-1}	96.6	2024[3]
Cu_2O/$Cu(OH)_2$ heterostructure	0.1 M KOH 500 ppm KNO_3	1.63 mg h^{-1} mg_{cat}^{-1}	76.95	2024[4]
Au nanorod@Cu_2O-Au nanoparticles	0.5 M Na_2SO_4 200 ppm KNO_3	3.4 mg h^{-1} mg_{cat}^{-1}	78.48	2023[5]
Cu_7Ni_3 ordered mesoporous carbon	0.1 M PBS 500 ppm KNO_3	0.237 mg h^{-1} mg_{cat}^{-1}	78.9	2023[6]
Cu nanosheets	1 M KOH 0.2 M KNO_3	10.57 mg h^{-1} mg_{cat}^{-1}	88	2023[7]
In−Pd bimetallene	0.5 M Na_2SO_4 0.1 M $NaNO_3$	13.7 mg h^{-1} mg_{cat}^{-1}	87.2	2023[8]
Co_3O_4-nanosheets/Au-nanowires nanohybrids	0.5 M K_2SO_4 50 mM KNO_3	2.66 mg h^{-1} mg_{cat}^{-1}	97.76	2023[9]
Au/Cu single atom alloys	0.5 M Na_2SO_4 100 ppm $NaNO_3$	6.562 mg h^{-1} mg_{cat}^{-1}	99.69	2023[10]
Cu-N-C single-atom catalyst	0.1 M KOH 0.1 M KNO_3	3.375 mg h^{-1} mg_{cat}^{-1}	84.7	2022[11]
Pd-Cu_2O corner-etched octahedra	0.5 M K_2SO_4 50 ppm KNO_3	0.93 mg h^{-1} mg_{cat}^{-1}	96.6	2022[12]

Cu@Cu 2,3,6,7,10,11-hexahydroxytriphenylene	0.5 M Na_2SO_4 500 ppm KNO_3	3.68 mg h^{-1} mg_{cat}^{-1}	67.55	2022[13]
Fe single atom/C	0.1 M K_2SO_4 0.5 M KNO_3	20 mg h^{-1} mg_{cat}^{-1}	75	2021[14]

References

1. Ni, J.; Yan, J.; Li, F.; Qi, H.; Xu, Q.; Su, C.; Sun, L.; Sun, H.; Ding, J.; Liu, B., Atomic Co-P catalytic pair drives efficient electrochemical nitrate reduction to ammonia. Adv. Energy Mater., 2024, **14,** 2400065.

2. Li, J.; Valenza, R.; Haussener, S., In situ synthesis of Cu_xO/N doped graphdiyne with pyridine N configuration for ammonia production via nitrate reduction. Small, 2024, **20,** 2310467.

3. Luo, W.; Guo, Z.; Ye, L.; Wu, S.; Jiang, Y.; Xu, P.; Wang, H.; Qian, J.; Zhou, X.; Tang, H.; et al., Electrical-driven directed-evolution of copper nanowires catalysts for efficient nitrate reduction to ammonia. Small, 2024, **20,** 2311336.

4. Geng, J.; Ji, S., Boosting electrocatalytic nitrate reduction to ammonia via $Cu_2O/Cu(OH)_2$ heterostructures promoting electron transfer. Nano Res., 2024, **17,** 4898-4907.

5. Yu, X.; Du, S.; Xu, Z.; He, J.; Liu, F.; Wang, B.; Sun, S.; Tang, Y.; Zhao, K., Surface-enhanced bimetallic effect of Au-Pd by internal electromagnetic fields from $Au@Cu_2O$ for efficient electrochemical nitrate reduction to ammonia. Chem. Eng. J., 2023, **480,** 148152.

6. Zhao, J.; Liu, L.; Yang, Y.; Liu, D.; Peng, X.; Liang, S.; Jiang, L., Insights into electrocatalytic nitrate reduction to ammonia via Cu-based bimetallic catalysts. ACS Sustainable Chem. Eng., 2023, **11,** 2468-2475.

7. Fu, Y.; Wang, S.; Wang, Y.; Wei, P.; Shao, J.; Liu, T.; Wang, G.; Bao, X., Enhancing electrochemical nitrate reduction to ammonia over Cu nanosheets via facet tandem catalysis. Angew. Chem. Int. Ed., 2023, **62,** e202303327.

8. Xie, M.; Tang, S.; Li, Z.; Wang, M.; Jin, Z.; Li, P.; Zhan, X.; Zhou, H.; Yu, G., Intermetallic single-atom alloy In-Pd bimetallene for neutral electrosynthesis of ammonia from nitrate. J. Am. Chem. Soc., 2023, **145,** 13957-13967.

9. Zhang, Z. N.; Hong, Q. L.; Wang, X. H.; Huang, H.; Li, S. N.; Chen, Y., Au nanowires decorated ultrathin Co_3O_4 nanosheets toward light-enhanced nitrate electroreduction. Small, 2023, **19,** 2300530.

10. Yin, H.; Peng, Y.; Li, J., Electrocatalytic reduction of nitrate to ammonia via a Au/Cu single atom alloy catalyst. Environ. Sci. Technol., 2023, **57,** 3134-3144.

11. Yang, J.; Qi, H.; Li, A.; Liu, X.; Yang, X.; Zhang, S.; Zhao, Q.; Jiang, Q.; Su, Y.; Zhang, L.; et al., Potential-driven restructuring of Cu single atoms to nanoparticles for boosting the electrochemical reduction of nitrate to ammonia. J. Am. Chem. Soc., 2022, **144,** 12062-12071.

12. Xu, Y.; Ren, K.; Ren, T.; Wang, M.; Wang, Z.; Li, X.; Wang, L.; Wang, H., Ultralow-content Pd in-situ incorporation mediated hierarchical defects in corner-etched Cu_2O octahedra for enhanced electrocatalytic nitrate reduction to ammonia. Appl. Catal., B, 2022, **306,** 121094.

13. Zhu, X.; Huang, H.; Zhang, H.; Zhang, Y.; Shi, P.; Qu, K.; Cheng, S.-B.; Wang, A.-L.; Lu, Q., Filling mesopores of conductive metal-organic frameworks with Cu clusters for selective nitrate reduction to ammonia. ACS Appl. Mater. Interfaces, 2022, **14,** 32176-32182.

14. Wu, Z.-Y.; Karamad, M.; Yong, X.; Huang, Q.; Cullen, D. A.; Zhu, P.; Xia, C.; Xiao, Q.; Shakouri, M.; Chen, F.-Y.; et al., Electrochemical ammonia synthesis via nitrate reduction on Fe single atom catalyst. Nat. Commun., 2021, **12,** 2870.